Dalton Transactions

ROYAL SOCIETY OF CHEMISTRY

PAPER

View Article Online
View Journal | View Issue

Cite this: *Dalton Trans.*, 2026, **55**, 6944

Synthesis of a rhenium(VII) trioxo complex supported by a triphyrin ligand: oxygenation chemistry and deposition on Au(111)

Manh Linh Nguyen,[a] Thomas Strunskus,[b] Christian Näther,[a] Jan Krahmer[a] and Felix Tuczek *[a]

Received 11th February 2026,
Accepted 14th April 2026

DOI: 10.1039/d6dt00370b

rsc.li/dalton

A new [14]triphyrin(2.1.1) ligand (TriP^{Et}, **1**) is synthesized, and its rhenium(I) and rhenium(VII) complexes [Re(TriP^{Et})(CO)$_3$] (**2**) and [ReO$_3$(TriP^{Et})] (**3**) are characterized in the bulk and on Au(111) surfaces. Self-assembled monolayers on Au(111) are prepared *via* wet-chemical deposition. IRRAS, supported by DFT, reveals a shift of the carbonyl stretching modes to higher wavenumbers, indicating an electron-withdrawing effect of the gold surface. On the other hand, XPS measurements of a monolayer of **3** show a reduction to Re(VI). A tilted adsorption geometry is observed, with reduced tilt compared to previous systems due to a shortening of the alkyl chains. Catalytic studies show that **3** promotes oxygen-transfer reactions, efficiently oxidizing triphenylphosphine with *N*-oxides and, more slowly, with molecular oxygen. While **3** is inactive for TBHP-mediated epoxidation of cyclooctene, irradiation in the presence of cyclooctene and oxygen leads to cyclooct-2-ene-hydroperoxide, indicating photooxygenation activity attributable to the complex, as the free ligand **1** decomposes under irradiation.

Introduction

With nearly 90% of all chemical products undergoing at least one catalytic step,[1] catalysts play a central role in industrial chemical processes. The development of new catalysts with higher efficiency thus remains highly desirable. A growing research area that aims to integrate the advantages of both homogeneous and heterogeneous catalysis is the heterogenization of homogeneous catalysts.[2–7] The concept behind this approach is to combine the beneficial properties of homogeneous and heterogeneous systems by immobilizing homogeneous catalysts on solid supports, either physically or chemically. This way the high selectivity and mild reaction conditions characteristic of homogeneous catalysts are preserved while also maintaining the efficient separation and recyclability associated with heterogeneous systems.

Along these lines Gottfried *et al.* employed well-studied planar metalloporphyrins as adsorbates for surface functionalization.[8–10] However, their studies revealed that porphyrin-type complexes when adsorbed on metal surfaces display low reactivities toward gaseous molecules. In a flat-lying geometry the close proximity of the metal center to the surface greatly limits its ability to coordinate additional ligands. This phenomenon is known in surface organometallic chemistry as "surface *trans* effect", leading to reduced accessibility and, therefore, reactivity of the metal center. A promising approach to mitigate this limitation involves reducing the size of the macrocycle, thereby lifting the metal center above the ligand plane and increasing its distance from the surface (Fig. 1). Subporphyrinoid complexes are particularly attractive in this context. Their inherent dome-shaped geometry offers a more accessible coordination environment for gaseous molecules, potentially enabling surface reactivity that is not achievable with conventional planar systems. In previous work, we identified the [14]triphyrin(2.1.1) (TriP) ligand originally reported by Yamada *et al.* as a promising ligand framework capable of supporting such geometries.[11–13]

A central challenge of the described project, as an initial step toward heterogenization, is the identification of a catalyst

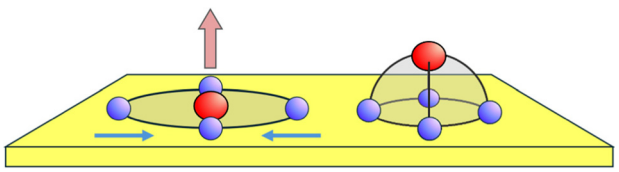

Fig. 1 Introducing the concept of surface-deposited, dome shaped catalysts: by reducing the size of the macrocycle of the macrocylcle a small gap between the metal center and metal surface is induced.

[a]*Institute of Inorganic Chemistry, Christian-Albrechts-University of Kiel, Max-Eyth-Straße 2, 24118 Kiel, Germany. E-mail: ftuczek@ac.uni-kiel.de*
[b]*Department of Material Science, Christian-Albrechts-University of Kiel, Kaiserstraße 1, 24143 Kiel, Germany*

that is active under homogeneous conditions and can be thoroughly characterized, followed by the question of whether such reactivity can be translated to surface-bound conditions. Initial attempts to coordinate the triphyrin ligand (TriP) to Ru(II) and Mn(I) led to catalytically inactive compounds, limiting their suitability for further investigation. Consequently, our focus shifted to high-valent rhenium. Since the discovery of methyltrioxorhenium (MTO) by Herrmann *et al.*,[14] rhenium complexes have attracted considerable attention due to their ability to activate small molecules such as O_2, CO, ethylene, and N_2 in solution.[15–18] In this context, oxygen activation and transfer reactions are of particular interest, as they may be transferable to surface chemistry with gaseous molecules such as O_2 and N_2O as oxidants.[19,20] Notably, our previous studies on the adsorption behavior of TriP complexes on metal surfaces revealed distinct adsorption differences depending on the deposition method. STM measurements of vacuum-evaporated (sub)monolayers of these molecules indicated a geometry nearly parallel to the surface.[21] By contrast, IRRAS, XPS, and NEXAFS measurements revealed that the Ru(II) complex $[RuCl(TriP)(CO)_2]$ deposited wet-chemically on Au(111) exhibits a tilted adsorption geometry.[22] We assumed that the flexible alkyl chains of the triphyrin ligand are the cause for this observation (Scheme 1).

Herein, we investigate the influence of shortened alkyl chains on the adsorption geometry of rhenium triphyrin complexes on surfaces as well as the accessibility of a corresponding high-valent rhenium species and its catalytic activity. To this end, we introduce a newly designed triphyrin ligand ($TriP^{Et}$, **1**) featuring shortened alkyl chains, followed by the synthesis of the derived carbonyl complex $[Re(TriP^{Et})(CO)_3]$ (**2**). Subsequent oxidation of **2** then leads to a novel trioxorhenium (VII) complex, $[ReO_3(TriP^{Et})]$ (**3**). Both **2** and **3** are characterized structurally and spectroscopically in the bulk and in thin surface-deposited films. As an initial step toward evaluating the suitability of complex **3** for heterogenized applications, its catalytic activity in selected oxygen-transfer reactions is examined in solution using various oxidants, including molecular oxygen. This approach provides us with a basis for future reactivity studies on surface-bound complex **3**.

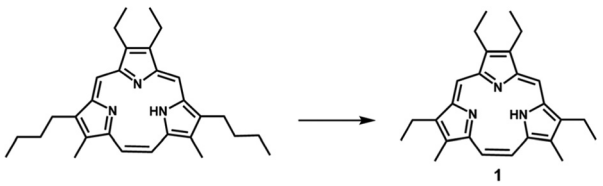

Scheme 1 The [14]triphyrin(2.1.1) (TriP) described by Yamada *et al.* and the new $TriP^{Et}$ (**1**) with shortened alkyl substituents introduced in this work.

Results and discussion

Syntheses of $TriP^{Et}$ (1), $[Re(TriP^{Et})(CO)_3]$ (2) & $[ReO_3(TriP^{Et})]$ (3)

As shown in Scheme 2, the synthesis of the ligand $TriP^{Et}$ (**1**) involves six steps, analogous to the procedure applied by Yamada *et al.* and Uno *et al.* to the synthesis of TriP.[11,23] Compounds **4**, **5**, **6**, and **7**, originally described by Johnson *et al.*, were prepared according to the process outlined by Uno *et al.*[23,24] Benzyl-3,5-dimethyl-4-ethylpyrrol-2-carboxylate (**4**) was obtained through a modified Knorr pyrrole synthesis starting from the corresponding α-amino-β-keto ester component

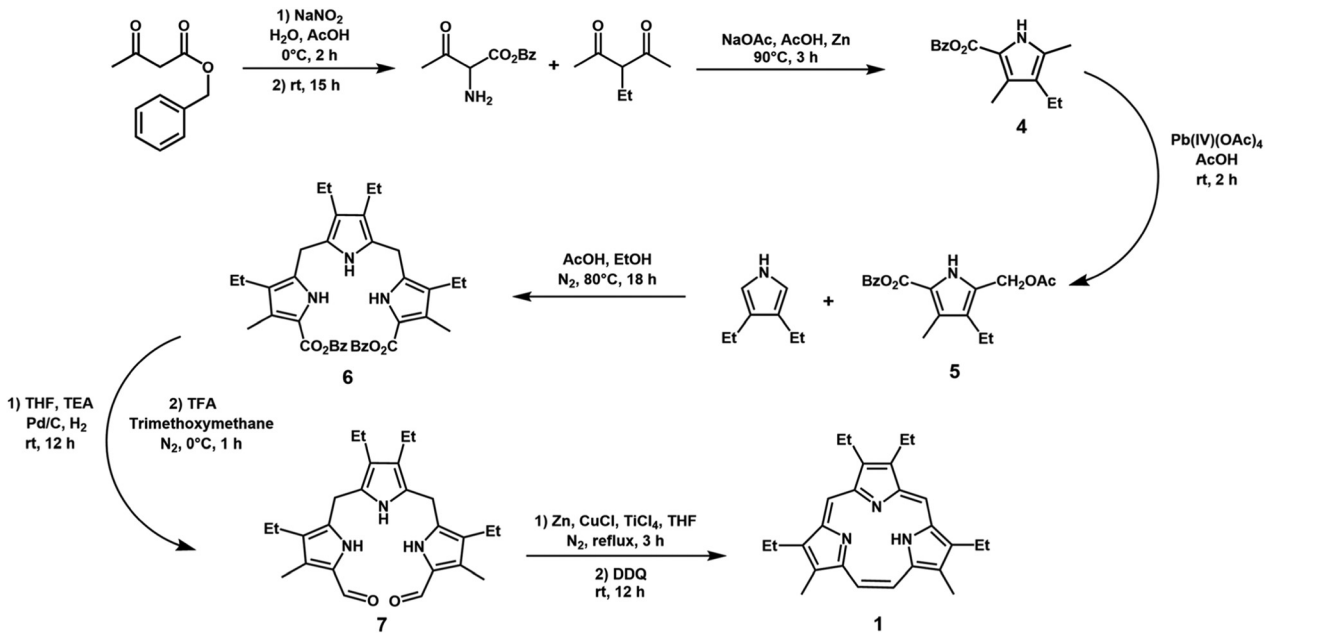

Scheme 2 Synthetic route of the [14]triphyrin(2.1.1) ($TriP^{Et}$, **1**) with shortened alkyl chains.

and 3-ethyl-2,4-pentanedione. The α-amino-β-keto ester was generated *in situ* by an amination reaction, after which the resulting precursor was acetylated using Pb(IV) acetate to yield the pyrrole building block **5**. Subsequent coupling with 3,4-diethylpyrrole afforded the tripyrrane (**6**).

The ester protecting group was removed by hydrogenolysis over Pd/C. The resulting intermediate was then formylated using trimethylformate in the presence of trifluoroacetic acid. Cyclization of the tripyrrane dialdehyde (**7**) proceeded *via* McMurry coupling, followed by oxidation with DDQ to produce TriP^{Et} (**1**) as a dark red solid with a yield of 31%. Complexation of **1** leading to [Re(TriP^{Et})(CO)$_3$] (**2**) was achieved by reaction with [ReCl(CO)$_5$] in the presence of sodium acetate as a deprotonating agent under reflux conditions (Scheme 3). The resulting Re(I) complex **2** is quite air-stable, demonstrating the need for a strong oxidant to achieve oxidation to higher valent species. Following the procedure reported by Furuta *et al.*, *tert*-butyl hydroperoxide (7 M in water, TBHP) was employed.[25] Conversion proceeded over several days, monitored by thin layer chromatography (TLC). The final product [ReO$_3$(TriP^{Et})] (**3**) was isolated as a bright red solid.

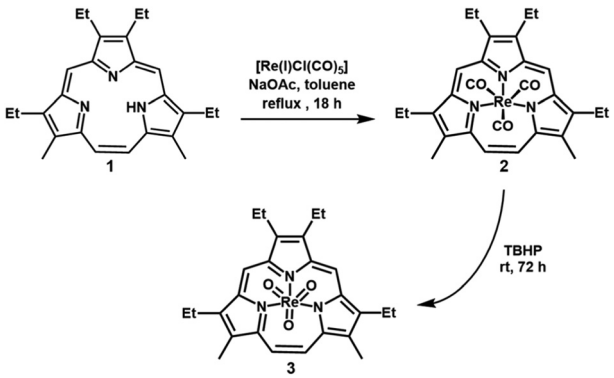

Scheme 3 Synthesis of [Re(TriP^{Et})(CO)$_3$] (**2**) and [ReO$_3$(TriP^{Et})] (**3**).

Crystals of **2** and **3** suitable for single crystal X-ray diffraction were obtained by dissolving the respective products in chloroform and allowing methanol (for **2**) or diethyl ether (for **3**) to diffuse slowly into the solutions. Structure analysis shows that both complexes adopt a slightly distorted octahedral geometry and display the expected dome-shaped triphyrin coordination (Fig. 2). In both structures, the rhenium center is positioned above the plane defined by the three inner nitrogen atoms, with Re–N bond lengths ranging from 2.121 Å for **2** to 2.185 Å for **3** (Table 1). This out-of-plane displacement reflects the intrinsic curvature of the triphyrin ligand. Comparison of the two complexes shows that the N–Re–N angles decrease from approximately 76° in **2** to 73° in **3**, corresponding to an average reduction of about 3°. This change can be attributed to an elongation of the Re–N bond lengths by approximately 0.048 Å upon conversion from **2** to **3**. As a result, the rhenium center in **3** exhibits a slightly more pronounced out-of-plane coordination environment. The Re–C bond lengths of **2**, approximately 1.93 Å, fall within the range typically observed for structurally related rhenium carbonyl complexes,[11] while the Re–O bond lengths in **3** average at 1.72 Å, in good agreement with reported values for high-valent rhenium oxo species.[26–28] Additional crystallographic data and CSD

Table 1 Selected bond lengths [Å] and angles [°] of [Re(TriPEt)(CO)$_3$] (**2**, top) and [ReO$_3$(TriPEt)] (**3**, bottom)

Re1–N1	2.1321(19)	N1–Re1–N2	80.95(7)
Re1–N2	2.1309(19)	N1–Re1–N3	76.33(7)
Re1–N3	2.1212(19)	N2–Re1–N3	76.83(7)
Re1–C31	1.926(2)	C31–Re1–N1	98.05(9)
Re1–C41	1.933(2)	C31–Re1–N3	171.32(8)
Re1–C51	1.931(2)	C31–Re1–C41	87.18(10)
Re1–N1	2.161(3)	N1–Re1–N2	73.49(10)
Re1–N2	2.185(3)	N1–Re1–N3	73.42(10)
Re1–N3	2.184(3)	N2–Re1–N3	76.33(10)
Re1–O1	1.727(3)	O1–Re1–N1	89.17(11)
Re1–O2	1.724(3)	O1–Re1–N3	159.13(11)
Re1–O3	1.719(2)	O1–Re1–O2	105.01(11)

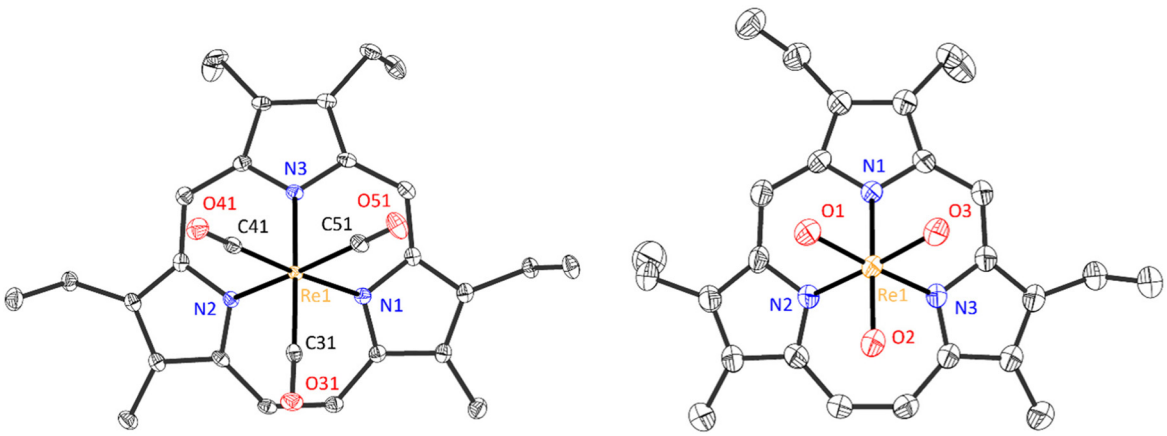

Fig. 2 Molecular structures of [Re(TriP^{Et})(CO)$_3$] (**2**) and [ReO$_3$(TriP^{Et})] (**3**) determined by single-crystal X-ray diffractometry. Ellipsoids are drawn at the 50% probability level.

numbers are provided in the SI and the relevant structural parameters are summarized in Table 1.

Oxygenation chemistry of [ReO_3(TriP^{Et})] (3)

Given the known reactivity of high-valent rhenium species, particularly Re(VII), we explored the catalytic properties of complex **3** in oxygenation reactions. Inspired by the work of Furuta *et al.*, its activity towards the oxidation of nucleophilic phosphines such as triphenylphosphine (PPh_3) was investigated first, employing molecular oxygen as well as the established 4-phenylpyridine-*N*-oxide as an activated oxygen species.[29]

As expected, the complex in combination with the oxidant 4-phenylpyridine-*N*-oxide efficiently converts triphenylphosphine to the corresponding phosphine oxides, which was followed with ^{31}P-NMR spectroscopy (Scheme 4, see SI for more information).[30] Notably, catalytic oxidation by **3** also proceeds under ambient atmosphere, showing faster conversion compared to just phosphine under air (Fig. 3).[31]

Then, the oxidation of cyclooctene was examined in the presence of **3** using H_2O_2 and *tert*-butyl hydroperoxide (THBP), but neither oxidant produced the corresponding epoxide. These results indicate that complex **3** is not suitable for this type of oxygenation. The same applies to molecular oxygen which did not lead to epoxidation in the presence of **3** either (Scheme 5).

Unexpected reactivity, however, emerged under photochemical conditions; *i.e.*, irradiation of cyclooctene at 365 nm in the presence of complex **3** under air led to the formation of cyclooct-2-ene hydroperoxide (Scheme 4). NMR quantitation revealed a turnover frequency of approximately 0.5 eq. per h under ambient conditions (see SI for more information). In the dark the hydroperoxide slowly decomposed to the corresponding alcohol, which is known for this class of compounds (Fig. 4).[32,33]

In order to account for these results, we first assumed that the observed catalytic activity of **3** is associated with a photooxygenation process involving the triphyrin ligand as a photosensitizer, consistent with the well-known photochemical properties of the structurally related porphyrins.[34–36] To check this hypothesis, the free ligand TriP^{Et} (**1**) was tested under identical conditions as applied for **3**. However, only ligand decomposition occurred, and no conversion of cyclooctene was observed. This shows that the TriP^{Et} system, in order to act as a photosensitizer, needs to be coordinated to a metal. Although the rhenium center may not be directly involved in the oxygenation, it plays an essential enabling role by stabilizing the TriP^{Et} ligand (**1**).

Scheme 4 Catalytic oxidation of triphenylphosphine (PPh_3) with 4-phenylpyridine-*N*-oxide/air and [ReO_3(TriP^{Et})] (**3**) as catalyst.

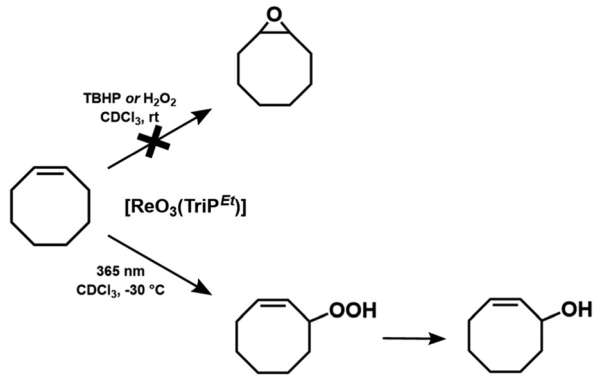

Scheme 5 Attempted conversion of cyclooctene to the corresponding epoxide and the photochemical conversion of cyclooctene to the peroxo acid with [ReO_3(TriP^{Et})] (**3**) as catalyst followed by the conversion of the hydroperoxide to the corresponding alcohol.

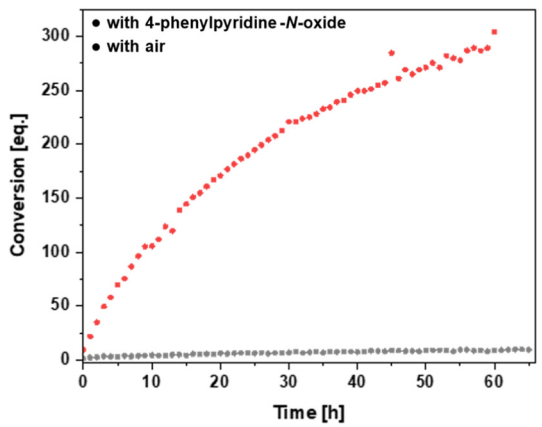

Fig. 3 Conversion over time of triphenylphosphine (PPh_3) with 4-phenylpyridine-*N*-oxide/air and [ReO_3(TriP^{Et})] (**3**) as catalyst.

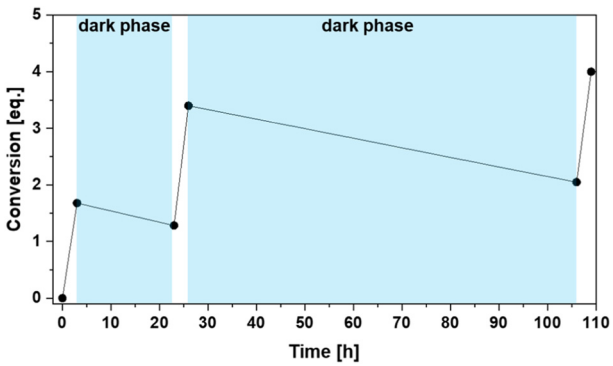

Fig. 4 Catalytic conversion of cyclooctene to cylooct-2-ene-hydroperoxide *vs.* time. The lighting phase average around 3 h per cycle while the lengths of the dark phase are indicated in the diagram.

The observation that the reaction besides the metal complex requires both irradiation with light and exposure to molecular oxygen can be accounted for by two mechanisms known from the literature on photooxygenations (Scheme 6).[37,38] In a Type I pathway, photoexcitation of the photosensitizer induces a single-electron transfer, generating a cyclooctene radical cation. The reduced photosensitizer transfers the electron to molecular oxygen, producing a superoxide radical anion. This reactive oxygen species subsequently reacts with the cyclooctene radical cation to form cyclooct-2-ene hydroperoxide which is observed as the primary reaction product in our experiments (see above).[39]

The Type II mechanism, which is more commonly described in the literature for olefin oxygenations and which we consider to be more likely in this case, involves energy transfer from the photoexcited complex to triplet oxygen ($^3O_2$) in solution, generating singlet oxygen ($^1O_2$).[40,41] The highly reactive $^1O_2$ then reacts with cyclooctene *via* an "ene"-type pathway, leading to the formation of the hydroperoxide product.

Deposition of [Re(TriP^{Et})(CO)$_3$] (2) on Au(111) and IRRA-spectroscopic investigation

Following the identification of catalytic activity for complex **3**, we turned our attention to its characterization on surfaces. Complexes **2** and **3** were deposited on Au(111) by immersing the gold substrate for one hour in 0.5 mM dichloromethane solutions of the respective complex, forming self-assembled monolayers. To evaluate the orientation of complexes supported by the TriP^{Et} ligand **1**, we focused first on the tricarbonyl rhenium complex **2**. Carbonyl ligands serve as excellent marker bands and are particularly suitable for infrared reflection absorption spectroscopy (IRRAS) analysis. Fig. 3 shows the IRRA spectrum of the adsorbed complex **2** together with the bulk IR spectrum and the corresponding simulated IRRA spectrum. The measured IRRA intensities, all approximately $\leq 10^{-3}$ absorbance units, confirm formation of a monolayer.[42–46] Due to the IRRAS surface selection rule, the relative signal intensities differ from those in the bulk IR spectrum, providing information about the molecular orientation on the surface. For the simulation, complex **2** was first modeled with the plane defined by the three pyrrolic nitrogen atoms parallel to the surface (*xy*-plane), omitting the gold substrate (Fig. 5).

As a reference for interpreting changes in electronic structure and orientation after adsorption, bulk IR data is essential.[42,47] In the bulk spectrum of **2**, three characteristic carbonyl stretching bands appear at 1996, 1878 and 1865 cm^{-1}. The totally symmetric vibration $A'(\mathbf{1})$ gives rise to the band at 1996 cm^{-1}. Regarding the vibrations of *E* parentage in C_{3v} symmetry, the band at 1865 cm^{-1} corresponds to

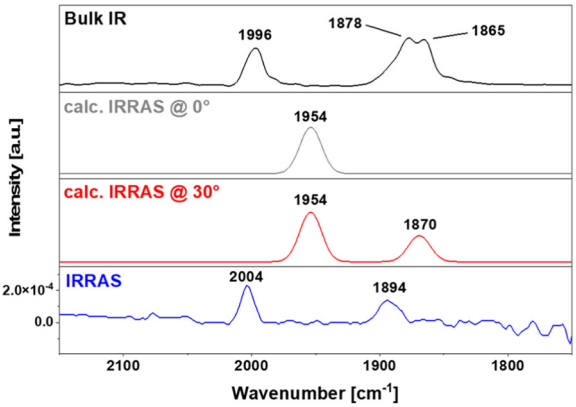

Fig. 5 Comparison of calculated and measured vibrational spectra of [Re(TriP^{Et})(CO)$_3$] (**2**) both in bulk material and after adsorption on Au(111) surfaces. The calculated tilted orientation corresponds to the complex **2** being inclined approximately 30° towards the *x*-axis.

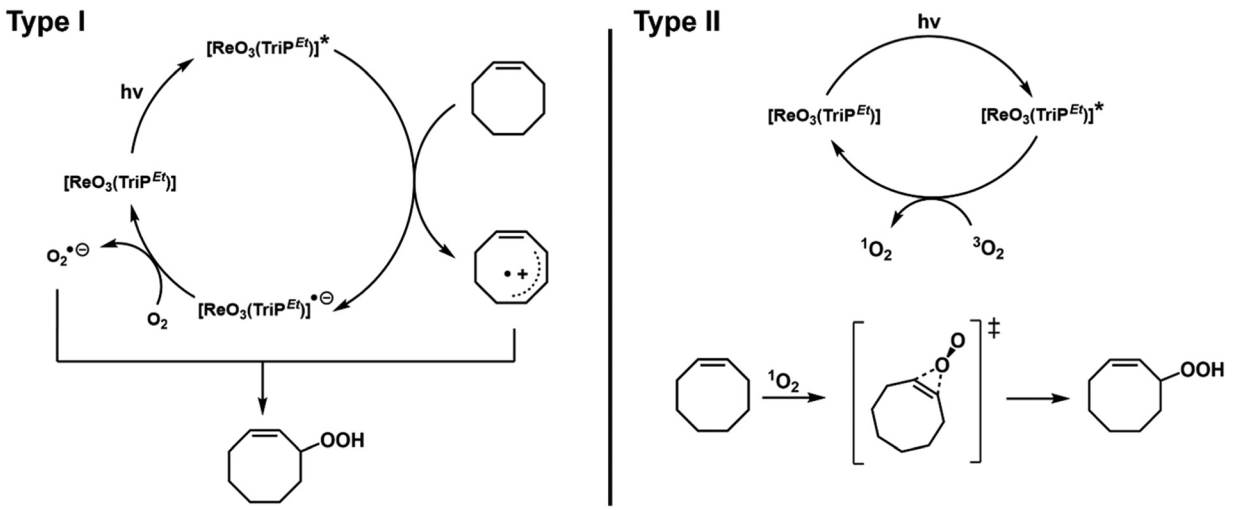

Scheme 6 Proposed mechanisms for the conversion of cyclooctene to cyclooct-2-ene-hydroperoxide with the Re(VII) trioxo complex **3** acting as a photosensitizer (see text).[37,38]

the out-of-phase CO mode (A'') and the band at 1878 cm^{-1} is assigned to the in-phase stretching mode $A'(2)$.

As observed in our previous study, the measured IRRA spectrum does not match the spectrum predicted for an adsorption geometry parallel to the surface (Fig. 5).[22] Consistent with a predominantly upright orientation, the intensity of the $A'(1)$ mode remains large; however, the intensities of the A'' and $A'(2)$ modes are only moderately diminished. According to the surface selection rule, the intensities of the A'' and $A'(2)$ vibrational modes should vanish for a strictly horizontal orientation. The fact that this is not observed indicates that the complex does not lie flatly on the surface. Because these two bands are very close in frequency, both in the experimental and simulated spectra, they appear as a single broadened feature, although two maxima can be recognized in the measured bulk IR spectrum (Fig. 5).

DFT-based simulations indicate an inclined adsorption geometry of **2** on Au(111) with a tilt angle of roughly 30°, reproducing the experimental intensities (Fig. 5). In our earlier study, the presence of flexible *n*-butyl chains in the original ligand (TriP) was identified as a likely cause of the pronounced tilt of nearly 60°.[22] These chains may interact with the solvent during adsorption, precluding an adsorption parallel to the surface. The resulting geometry appears to be retained after drying. Comparison of our previous and current results indicates that shortening the alkyl chains indeed reduces the degree of tilt (Fig. 6). This demonstrates a clear dependence of adsorption geometry on alkyl chain length and constitutes an improvement in orientational control.

In addition to information on the adsorption geometry, IRRAS provides insight into the electronic structure of the complex on the metal surface. In our earlier work, we showed that gold exhibits a strong electron-withdrawing effect, which manifests itself as a shift of carbonyl stretching vibrations to higher wavenumbers. This shift arises from static withdrawal of electron density from the metal center, strengthening the C–O bonds. In tricarbonyl complexes, we also identified a second phenomenon denominated as dynamic activation, in which the totally symmetric $A'(1)$ vibration dynamically withdraws electron density from the substrate.[42,44–46] Because of this charge modulation, the $A'(1)$ mode typically experiences a smaller surface-induced shift than the other two CO modes. The same behavior is observed here: upon adsorption on Au (111), the A'' and $A'(2)$ bands shift by approximately 21 cm^{-1} to higher wavenumbers, indicating strong static deactivation by the gold surface. In contrast, the $A'(1)$ mode only shifts by about 8 cm^{-1}, consistent with dynamic activation counteracting the electron-withdrawing effect of the substrate. Overall, the carbonyl vibrational pattern reflects the combined influence of static and dynamic (de)activation processes as previously reported on other surface-adsorbed complexes.[42]

The adsorption geometry of compound **3** and the influence of the gold substrate on its electronic structure were analyzed in a similar fashion. The bulk and surface IR data of $[ReO_3(TriP^{Et})]$ (**3**) are shown in Fig. 7.

In the bulk IR spectrum the totally symmetric vibration $A'(1)$ can be found at 928 cm^{-1} whereas the out-of-phase vibration A'' and the in-phase vibration $A'(2)$ are at 899 cm^{-1} and 885 cm^{-1}, respectively. Table 2 summarizes the Re=O vibrational frequencies of selected Re(VII) trioxo complexes reported in the literature. Comparison with complex **3** shows that the Re=O stretching modes lie well within a similar range, with deviations generally not exceeding approximately 20 cm^{-1}. The only notable exception is the highly catalytically active methyltrioxorhenium (MTO), which exhibits shifts to higher wavenumbers, with the $A'(1)$ mode observed at 1002 cm^{-1} and the A'' and $A'(2)$ modes being around 953 cm^{-1}.

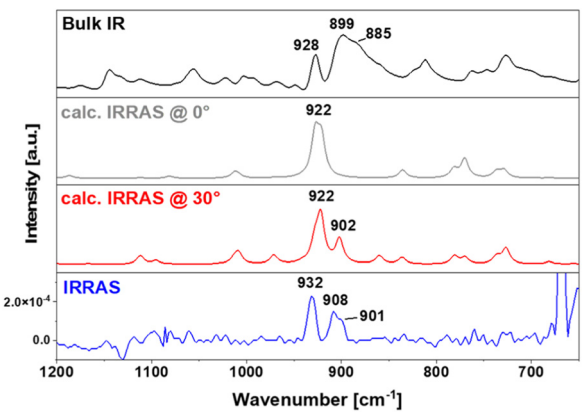

Fig. 7 Comparison of calculated and measured vibrational spectra of $[ReO_3(TriP^{Et})]$ (**3**) both in bulk material and after adsorption on Au(111) surfaces. The calculated tilted orientation corresponds to the complex **3** being inclined approximately 30° towards the *x*-axis.

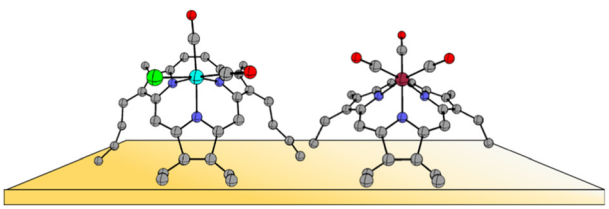

Fig. 6 Schematic comparison of the tilted geometry of $[Re(TriP^{Et})(CO)_3]$ (**2**) (right) with the shortened alkyl chains and the tilted geometry of the $[RuCl(TriP)(CO)_2]$ (left) with the original TriP backbone, previously reported, on the Au(111) surface.

Table 2 Comparison of experimental Re=O vibrational frequencies (cm^{-1}) of $[ReO_3(TriP^{Et})]$ (**3**) with selected rhenium trioxo complexes from literature

Compound	$A'(1)$	A''	$A'(2)$
$[ReO_3(TriP^{Et})]$ (**3**)	928	899	885
$[Re(CH_3)O_3]$ (MTO) [48]	1002	953	
$[Re(\eta^5\text{-}C_5H_5)O_3]$ [49]	926	886	
$[Re(NFP)O_3]$ [25]	932	908	
$[Re(tacn)O_3]Cl$ [50]	945	920	

As evident from the non-vanishing intensities of the A'' and $A'(2)$ modes, complex **3** does not adopt a parallel orientation on the Au(111) surface but instead assumes a tilted geometry, similar to **2**. Based on DFT calculations, the inclination angle has a value of approximately 30°, similar to **2**. Furthermore, we observed shifts of the metal-oxo vibrational frequencies in the surface-adsorbed monolayer of **3**. As described above, due to the electron withdrawing nature of gold the A'' and $A'(2)$ bands shift by approximately 7 cm^{-1} to higher wavenumbers. In contrast, the $A'(1)$ mode exhibits a smaller induced shift of 4 cm^{-1} than the other vibration modes consistent with dynamic activation partially compensating the electron-withdrawing effect of the substrate. The interaction of complex **3** with the gold substrate reflects an electron-withdrawing nature of the surface, leading to a shortening of the Re=O bonds.

Surface-spectroscopic investigations of [ReO_3(TriP^{Et})] (3) by XPS and NEXAFS

X-ray photoelectron spectroscopy (XPS) was employed to determine whether compounds **2** and **3** remain chemically intact and free of contamination after deposition onto Au(111). Since a major focus of this study is the potential catalytic reactivity of the high-valent Re complex **3** on surfaces, the corresponding spectra are discussed in detail in the following. The spectra of the free ligand **1** and tricarbonyl complex **2** are presented and discussed in the SI.

The survey spectrum of **3** (Fig. 8) displays the characteristic Au 4f peaks at 84.0 and 87.5 eV as well as Au 4d signals at 335.0 and 352.5 eV. A well-defined C 1s peak at 284.5 eV is also observed. The intensity ratio between the Au $4d_{5/2}$ and C 1s signals supports the formation of a monolayer on Au(111).[42–46]

Higher-resolution spectra of the N 1s, C 1s, O 1s, and Re 4f regions were recorded with acquisition times of up to one hour.

The XP spectra are shown for a thick layer (corresponding to bulk) in Fig. 8 and for a monolayer in Fig. 9. In the bulk XP spectra (Fig. 9a), two sets of Re 4f signals are observed at 47.6/45.2 eV (red) and 46.5/44.1 eV (blue), each showing the expected spin–orbit splitting of 2.4 eV and an intensity ratio of 4 : 3 corresponding to the $4f_{5/2}$ and $4f_{7/2}$ components. The relative ratio between the two species is around 73 : 27. The difference of 1.1 eV between the two species indicates the presence of Re(VII) at 45.2 eV, in agreement with literature values, and a

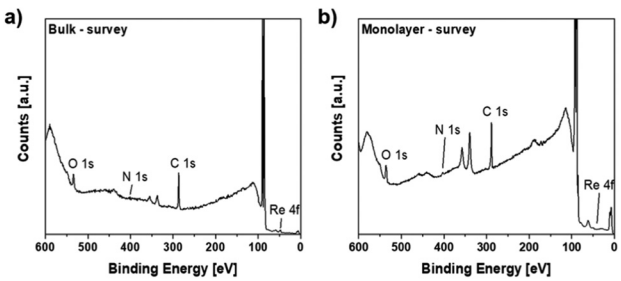

Fig. 8 Survey spectra of [ReO_3(TriP^{Et})] (**3**) in bulk form (a) and as a monolayer (b) on Au(111).

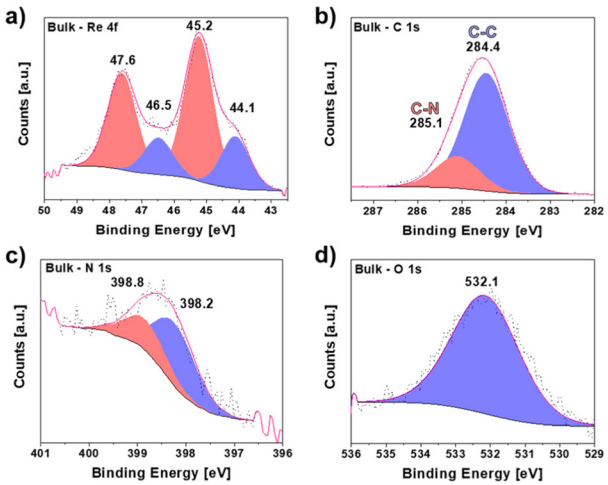

Fig. 9 XP spectra of Re 4f (a), C 1s (b), N 1s (c), and O 1s (d) for [ReO_3(TriP^{Et})] (**3**) as a thick layer on Au(111).

reduced Re(VI) species at 44.1 eV.[51–53] The formation of mixed-valent rhenium states, such as Re(VII)/Re(VI), is known for rhenium oxides like Re_2O_7. Rhenium oxides can undergo partial reduction under thermal treatment or X-ray exposure,[51,52,54] a behaviour that is highly relevant to the catalytic properties of Re(VII) oxide.[55] Despite this partial reduction, the ligand framework remains intact: the C 1s spectrum (Fig. 9b) shows an intensity ratio of 21 : 79 for C–N to C–C environments, close to the theoretical ratio of 23 : 77, and the N 1s spectrum exhibits two peaks at 398.2 and 398.8 eV in a 2 : 1 ratio (Fig. 9c) reflecting the two distinct nitrogen of the triphyrin backbone, similarly observed in free-base porphyrins.[22,56,57] Finally, the O 1s region contains a broad peak at 532.1 eV, consistent with coordinated oxygen (Fig. 9d).

The monolayer spectra (Fig. 10) closely resemble the bulk data with one notable exception that the Re centers now are

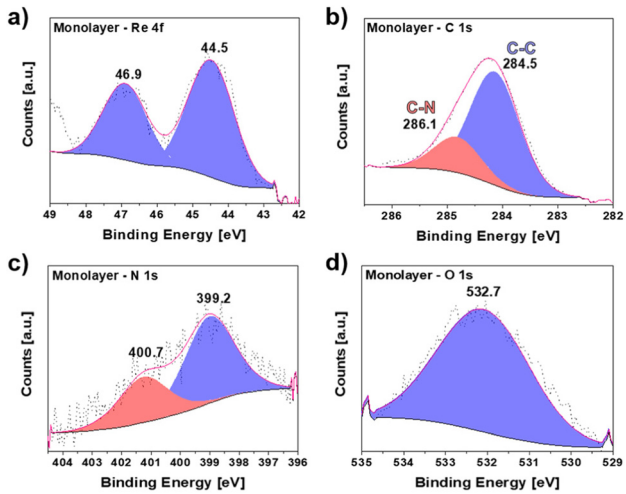

Fig. 10 XP spectra of Re 4f (a), C 1s (b), N 1s (c), and O 1s (d) for a monolayer of [ReO_3(TriP^{Et})] (**3**) on Au(111).

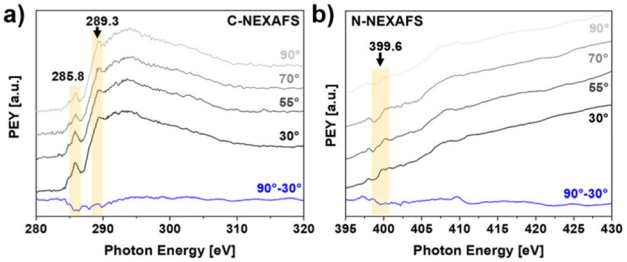

Fig. 11 Normalized NEXAFS spectra at the C (a) and N K-edges (b) of [ReO_3(TriP^{Et})] (**3**) as a monolayer on Au(111) measured at incident angles of 30°, 55°, 70° and 90°.

fully one-electron reduced to Re(VI). This behavior is certainly due to the greater exposure of the surface-bound species to X-ray irradiation whereas the Re complexes in the bulk material are partially shielded by outer layers. Importantly, the relative C 1s intensities in the monolayer match with a ratio of 23 : 77 perfectly with the thick layer and the theoretical values, thus confirming that the triphyrin ligand remains unaffected by the reduction of the metal center. Overall, the data indicate that compound **3** forms a chemically intact monolayer on Au (111), with only the metal centers undergoing reduction under the conditions of the XPS experiment.

To further investigate the adsorption geometry of compound **3**, near-edge X-ray absorption fine structure (NEXAFS) spectroscopy was employed. Spectra at the carbon and nitrogen K-edges were measured for a monolayer of [ReO_3(TriP^{Et})] (**3**) on Au(111) at various angles of incidence (Fig. 11a and b).

Oxygen 1s photoelectron spectra were also measured; however, the corresponding NEXAFS spectra did not provide meaningful orientational information due to residual water on the Au(111) surface despite preparation under dry conditions. For this reason, they are not included in the analysis.

The C K-edge spectrum (Fig. 11a) features two prominent π* resonances. Based on literature data and structurally related systems, the resonances at 285.8 eV and 289.3 eV are assigned to C 1s → π* transitions of the pyrrole units.[22,58–60] These transitions exhibit only weak angular dependence, with relatively minor changes in intensity between 30° and 90°. The nitrogen K-edge spectrum (Fig. 11b) displays a single π* resonance at 399.5 eV, corresponding to the N 1s → π* transition of the pyrrole nitrogen atoms.[58,59] Similar to the carbon K-edge, this transition shows only a slight decrease in intensity with increasing angle of incidence. Notably, a non-vanishing intensity remains at 90°, indicating that the pyrrole rings are not perfectly parallel to the surface but adopt a tilted orientation. These observations are in agreement with the IRRAS data discussed above and confirm a tilted adsorption geometry of complex **3** on the gold surface.

Conclusions

In this study, the [14]triphyrin(2.1.1) ligand TriP^{Et} (**1**) as well as the corresponding rhenium(I) and rhenium(VII) triphyrin complexes [Re(TriP^{Et})(CO)$_3$] (**2**) and [ReO_3(TriP^{Et})] (**3**) were synthesized and thoroughly characterized both in the bulk and adsorbed on Au(111) surfaces. Single-crystal X-ray diffraction confirmed the anticipated dome-shaped geometry of both complexes, demonstrating successful metal coordination.

Catalytic investigations revealed that the Re(VII) trioxo complex **3** in homogeneous solution is capable of oxygen-transfer reactions regarding the oxidation of triphenylphosphine using mild oxidants such as *N*-oxides and, albeit more slowly, molecular oxygen. While attempts to use **3** as a catalyst for the epoxidation of cyclooctene with TBHP were unsuccessful, irradiation of complex **3** in the presence of cyclooctene and molecular oxygen resulted in the formation of cyclooct-2-ene-hydroperoxide which subsequently decomposes to the corresponding alcohol. This photooxygenation activity was attributed to **3** acting as a photosensitizer, the free ligand **1** alone being unable to promote the conversion.

Self-assembled monolayers on Au(111) were prepared *via* wet-chemical deposition. IRRAS measurements revealed consistent shifts of the carbonyl- and oxo stretching frequencies by approximately 8 and 21 cm^{-1} and 4 and 7 cm^{-1}, respectively, to higher wavenumbers, indicating that dynamic activation and static (de)activation are the primary electronic influences on the surface-bound complexes, consistent with observations in related systems. Moreover, IRRAS data, supported by DFT calculations, suggested a tilted adsorption geometry relative to the surface plane, deviating from a fully parallel orientation. Comparison with our previous results shows that shortening the alkyl chains reduces the degree of tilt, confirming a clear dependence of adsorption geometry on alkyl chain length and demonstrating improved orientational control.

With the catalytic activity of **3** in solution being demonstrated and its structural integrity on a Au(111) surface confirmed, the reactivity of **3** on surfaces can now be addressed. In this context, Kazansky *et al.* reported that surface-dispersed Re(VII) oxides can be activated for oxygen transfer *via* partial reduction induced by X-ray irradiation, leading to increased catalytic yields.[54] Consistent with this behavior, our XPS experiments on **3** indicate the formation of a reduced rhenium species assigned to Re(VI). Although no conclusions can be drawn from these experiments regarding possible structural changes, the ratio of the carbon species from the C 1s spectra indicate an intact ligand **1** framework, suggesting that no decomposition occurs upon X-ray irradiation of **3**. Based on these results it might be possible that exposure of **3** to UV light could (at least, transiently) generate a Re(VI) oxo (or oxyl) species in which at least one the Re=O bonds is weakened, analogous to the irradiation of **3** with X-ray irradiation. Such a species may then be able to react with hydrocarbons, eventually leading to oxidation or oxygenation of these compounds.

Author contributions

Manh Linh Nguyen: writing – original draft, visualization, investigation, validation. Thomas Strunskus: project adminis-

tration. Christian Näther: formal analysis. Jan Krahmer: formal analysis. Felix Tuczek: supervision, writing – review & editing.

Conflicts of interest

There are no conflicts to declare.

Data availability

The data supporting this article have been included as part of the supplementary information (SI). Supplementary information is available. See DOI: https://doi.org/10.1039/d6dt00370b.

CCDC 2530155–2530157 (**2**, **3**, **3-Et$_2$O**) contain the supplementary crystallographic data for this paper.[61a–c]

Acknowledgements

The authors would like to thank the Helmholtz-Zentrum Berlin (HZB) for providing beamtime at the BESSY II/HE-SGM for XPS and NEXAFS measurements, particularly Dr Maria Brzhezinskaya. Special thanks also go to the spectroscopic departments at the institutes of inorganic and organic chemistry for their assistance with measurements. The authors are also grateful for the financial support provided by the CAU Kiel.

References

1 J. J. Bravo-Suárez, R. V. Chaudhari and B. Subramaniam, *Novel Materials for Catalysis and Fuels Processing*, American Chemical Society, Washington, DC, 2013.
2 J. C. Bailar, *Cat. Rev. – Sci. Eng.*, 1974, **10**, 17–36.
3 A. E. C. Collis and I. T. Horváth, *Catal. Sci. Technol.*, 2011, **1**, 912.
4 M. K. Samantaray, S. K. Mishra, A. Saidi and J.-M. Basset, *J. Organomet. Chem.*, 2021, **945**, 121864.
5 M. K. Samantaray, E. Pump, A. Bendjeriou-Sedjerari, V. D'Elia, J. D. A. Pelletier, M. Guidotti, R. Psaro and J.-M. Basset, *Chem. Soc. Rev.*, 2018, **47**, 8403–8437.
6 C. H. Mak, X. Han, M. Du, J.-J. Kai, K. F. Tsang, G. Jia, K.-C. Cheng, H.-H. Shen and H.-Y. Hsu, *J. Mater. Chem. A*, 2021, **9**, 4454–4504.
7 S. A. Johnson, J. R. Wilkes, D. Wang and J. A. Byers, *ACS Catal.*, 2024, **14**, 18535–18541.
8 J. M. Gottfried, *Surf. Sci. Rep.*, 2015, **70**, 259–379.
9 J. M. Gottfried, K. Flechtner, A. Kretschmann, T. Lukasczyk and H.-P. Steinrück, *J. Am. Chem. Soc.*, 2006, **128**, 5644–5645.
10 W. Hieringer, K. Flechtner, A. Kretschmann, K. Seufert, W. Auwärter, J. V. Barth, A. Görling, H.-P. Steinrück and J. M. Gottfried, *J. Am. Chem. Soc.*, 2011, **133**, 6206–6222.
11 D. Kuzuhara, H. Yamada, Z. Xue, T. Okujima, S. Mori, Z. Shen and H. Uno, *Chem. Commun.*, 2011, **47**, 722–724.
12 S. Shimizu, *Chem. Rev.*, 2017, **117**, 2730–2784.
13 D. Prasannan and M. Ravikanth, *Coord. Chem. Rev.*, 2020, **407**, 213172.
14 F. E. Kühn, A. Scherbaum and W. A. Herrmann, *J. Organomet. Chem.*, 2004, **689**, 4149–4164.
15 T. Chatterjee and M. Ravikanth, *Coord. Chem. Rev.*, 2020, **422**, 213480.
16 J. R. Dilworth, *Coord. Chem. Rev.*, 2021, **436**, 213822.
17 A. Gradenegger, J. A. Schachner, F. Belaj and N. C. Mösch-Zanetti, *RSC Adv.*, 2024, **14**, 40058–40068.
18 G. Rouschias, *Chem. Rev.*, 1974, **74**, 531–566.
19 A. Podgorsek, M. Zupan and J. Iskra, *Angew. Chem., Int. Ed.*, 2009, **48**, 8424–8450.
20 Z. Shi, C. Zhang, C. Tang and N. Jiao, *Chem. Soc. Rev.*, 2012, **41**, 3381–3430.
21 X. Meng, M. L. Nguyen, A. Weismann, C. Li, F. Tuczek and R. Berndt, *J. Phys. Chem. C*, 2023, **127**, 12118–12124.
22 M. L. Nguyen, K. Yildiz, N. Michaelis, K. U. Clausen, T. Strunskus, C. Näther and F. Tuczek, *Z. Anorg. Allg. Chem.*, 2025, **651**, e202500143.
23 H. Uno, K.-I. Nakamoto, K. Kuroki, A. Fujimoto and N. Ono, *Chem. – Eur. J.*, 2007, **13**, 5773–5784.
24 J. L. Sessler, M. R. Johnson and V. Lynch, *J. Org. Chem.*, 1987, **52**, 4394–4397.
25 M. Toganoh, S. Ikeda and H. Furuta, *Chem. Commun.*, 2005, 4589–4591.
26 M. Toganoh and H. Furuta, *Chem. Lett.*, 2005, **34**, 1034–1035.
27 D. D. DuMez and J. M. Mayer, *Inorg. Chem.*, 1998, **37**, 445–453.
28 S. Raju, C. A. M. R. van Slagmaat, J. Li, M. Lutz, J. T. B. H. Jastrzebski, M.-E. Moret and R. J. M. Klein Gebbink, *Organometallics*, 2016, **35**, 2178–2187.
29 M. Toganoh, S. Ikeda and H. Furuta, *Inorg. Chem.*, 2007, **46**, 10003–10015.
30 M. Toganoh, K. Fujino, S. Ikeda and H. Furuta, *Tetrahedron Lett.*, 2008, **49**, 1488–1491.
31 K. U. Clausen, N. Pienack, J. Gripp and F. Tuczek, *Chem. – Eur. J.*, 2024, **30**, e202304359.
32 R. R. Hiatt, T. Mill and F. R. Mayo, *J. Org. Chem.*, 1968, **33**, 1416–1420.
33 R. W. Denny and A. Nickon, *Sensitized Photooxygenation of Olefins*, Wiley, New York, 1973.
34 M. DeRosa and R. J. Crutchley, *Coord. Chem. Rev.*, 2002, **233–234**, 351–371.
35 M. Hajimohammadi, F. Bahadoran, S. S. H. Davarani and N. Safari, *React. Kinet. Mech. Catal.*, 2010, **99**, 243–250.
36 M. Hajimohammadi and N. Safari, *J. Porphyrins Phthalocyanines*, 2010, **14**, 639–645.
37 M. S. Baptista, J. Cadet, P. Di Mascio, A. A. Ghogare, A. Greer, M. R. Hamblin, C. Lorente, S. C. Nunez, M. S. Ribeiro, A. H. Thomas, M. Vignoni and T. M. Yoshimura, *Photochem. Photobiol.*, 2017, **93**, 912–919.
38 C. Bian, A. K. Singh, L. Niu, H. Yi and A. Lei, *Asian J. Org. Chem.*, 2017, **6**, 386–396.

39 D. S. Steichen and C. S. Foote, *J. Am. Chem. Soc.*, 1981, **103**, 1855–1857.
40 A. Greer, *Acc. Chem. Res.*, 2006, **39**, 797–804.
41 M. Orfanopoulos, *Photochem. Photobiol.*, 2021, **97**, 1182–1218.
42 A. Schlimm, N. Stucke, B. M. Flöser, T. Rusch, J. Krahmer, C. Näther, T. Strunskus, O. M. Magnussen and F. Tuczek, *Chem. – Eur. J.*, 2018, **24**, 10732–10744.
43 F. Petersen, I. Lautenschläger, A. Schlimm, B. M. Flöser, H. Jacob, R. Amirbeigiarab, T. R. Rusch, T. Strunskus, O. Magnussen and F. Tuczek, *Dalton Trans.*, 2021, **50**, 1042–1052.
44 K. U. Clausen, A. Schlimm, K. Bedbur, C. Näther, T. Strunskus, L. Fu, M. Gruber, R. Berndt and F. Tuczek, *Chem. – Eur. J.*, 2024, **30**, e202303912.
45 K. U. Clausen, X. Meng, K. Reisig, C. Näther, T. Strunskus, R. Berndt and F. Tuczek, *Dalton Trans.*, 2024, **53**, 18304–18312.
46 F. Tuczek, K. Yildiz, K. U. Clausen, C. Näther and T. Strunskus, *ChemPlusChem*, 2025, e202500274.
47 Y. J. Chabal, *Surf. Sci. Rep.*, 1988, **8**, 211–357.
48 W. A. Herrmann, J. G. Kuchler, J. K. Felixberger, E. Herdtweck and W. Wagner, *Angew. Chem., Int. Ed. Engl.*, 1988, **27**, 394–396.
49 É. Bencze, J. Mink, C. Németh, W. Herrmann, B. Lokshin and F. Kühn, *J. Organomet. Chem.*, 2002, **642**, 246–258.
50 K. Wieghardt, C. Pomp, B. Nuber and J. Weiss, *Inorg. Chem.*, 1986, **25**, 1659–1661.
51 W. T. Tysoe, F. Zaera and G. A. Somorjai, *Surf. Sci.*, 1988, **200**, 1–14.
52 H. Yao and M. Shelef, *J. Catal.*, 1976, **44**, 392–403.
53 M. Zubkins, A. Sarakovskis, E. Strods, L. Bikse, B. Polyakov, A. Kuzmin, V. Vibornijs and J. Purans, *Mater. Chem. Phys.*, 2022, **289**, 126399.
54 A. Tarasov, B. Shelimov, V. Kazansky and J. Mol, *J. Mol. Catal. A: Chem.*, 1997, **115**, 219–228.
55 C. C. Romão, F. E. Kühn and W. A. Herrmann, *Chem. Rev.*, 1997, **97**, 3197–3246.
56 J. P. Macquet, M. M. Millard and T. Theophanides, *J. Am. Chem. Soc.*, 1978, **100**, 4741–4746.
57 D. H. Karweik and N. Winograd, *Inorg. Chem.*, 1976, **15**, 2336–2342.
58 T. Okajima, Y. Yamamoto, Y. Ouchi and K. Seki, *J. Electron. Spectrosc. Relat. Phenom.*, 2001, **114–116**, 849–854.
59 N. Schmidt, R. Fink and W. Hieringer, *J. Chem. Phys.*, 2010, **133**, 54703.
60 M. Turner, O. P. H. Vaughan, G. Kyriakou, D. J. Watson, L. J. Scherer, A. C. Papageorgiou, J. K. M. Sanders and R. M. Lambert, *J. Am. Chem. Soc.*, 2009, **131**, 14913–14919.
61 (*a*) CCDC 2530155: Experimental Crystal Structure Determination, 2026, DOI: 10.5517/ccdc.csd.cc2qxtxd; (*b*) CCDC 2530156: Experimental Crystal Structure Determination, 2026, DOI: 10.5517/ccdc.csd.cc2qxtyf; (*c*) CCDC 2530157: Experimental Crystal Structure Determination, 2026, DOI: 10.5517/ccdc.csd.cc2qxtzg.